LETTER

doi:10.1038/nature09866

Controlling inelastic light scattering quantum pathways in graphene

Chi-Fan Chen[1], Cheol-Hwan Park[1], Bryan W. Boudouris[2,3], Jason Horng[1], Baisong Geng[1], Caglar Girit[1], Alex Zettl[1,3], Michael F. Crommie[1,3], Rachel A. Segalman[2,3], Steven G. Louie[1,3] & Feng Wang[1,3]

Inelastic light scattering spectroscopy has, since its first discovery[1,2], been an indispensable tool in physical science for probing elementary excitations, such as phonons[3], magnons[4] and plasmons[5] in both bulk and nanoscale materials. In the quantum mechanical picture of inelastic light scattering, incident photons first excite a set of intermediate electronic states, which then generate crystal elementary excitations and radiate energy-shifted photons[6]. The intermediate electronic excitations therefore have a crucial role as quantum pathways in inelastic light scattering, and this is exemplified by resonant Raman scattering[6] and Raman interference[7,8]. The ability to control these excitation pathways can open up new opportunities to probe, manipulate and utilize inelastic light scattering. Here we achieve excitation pathway control in graphene with electrostatic doping. Our study reveals quantum interference between different Raman pathways in graphene: when some of the pathways are blocked, the one-phonon Raman intensity does not diminish, as commonly expected, but increases dramatically. This discovery sheds new light on the understanding of resonance Raman scattering in graphene. In addition, we demonstrate hot-electron luminescence[9] in graphene as the Fermi energy approaches half the laser excitation energy. This hot luminescence, which is another form of inelastic light scattering, results from excited-state relaxation channels that become available only in heavily doped graphene.

Graphene, a two-dimensional carbon sheet[10,11], is an attractive system in which to explore novel inelastic light scattering phenomena. Raman scattering from few-layer graphene is readily observable, and has been widely used to distinguish layer thickness[12], characterize quality[13–15], and probe electron–phonon interactions[16,17]. At the same time, graphene has unique optical transitions that can be tuned through electrostatic gating[18–20]. However, using electrostatic doping to control quantum pathways of inelastic light scattering has presented a challenge, because it requires the modification of intermediate excited states with transition energies close to the laser photon energy. Here we achieve this goal by combining highly efficient ion-gel gating (Methods) and near-infrared laser excitation. This combination enables us to control intermediate optical transition pathways and reveal interesting new optical phenomena. We show that, counter-intuitively, the one-phonon Raman signal increases dramatically when certain quantum pathways are blocked. This represents a notable manifestation of quantum interference between different Raman scattering pathways. On the other hand, the two-phonon Raman signal decreases monotonically with reduced quantum channels. In addition, we observe the emergence of hot luminescence[9] when the Fermi energy (E_F) approaches half the value of the photon excitation energy. This hot luminescence in graphene arises from new dynamic relaxation channels of the photo-excited states.

The excitation pathways in graphene samples are controlled through electrostatic doping using a high-capacitance ion-gel gate dielectric[21,22]. Figure 1a displays a diagram of a typical device. The carrier concentration in graphene is controlled by the top gate voltage (V_g). The doping dependence of electrical transport, optical transmission and inelastic light scattering are measured on the same graphene devices. Figure 1b shows the electrical resistance curve of a graphene device, which has a charge neutral point (CNP) at 1.2 V. The resistance decreases from the CNP value on both electron and hole doping. A lower resistance, corresponding to a higher carrier concentration and a larger shift of Fermi energy, is achieved in the hole-doping region; such hole doping in graphene will be the focus of our study.

To determine the gate-induced Fermi energy shift in graphene samples, we use infrared transmission spectroscopy[18,19]. This approach is based on the fact that an optical transition can be blocked by hole doping when the initial state has an energy higher than the Fermi level and is not occupied (Fig. 1c). Figure 1d displays the gate-induced change in the real part of graphene optical conductivity ($\Delta\sigma'$) at different gate biases. The spectra exhibit distinct step-like behaviour,

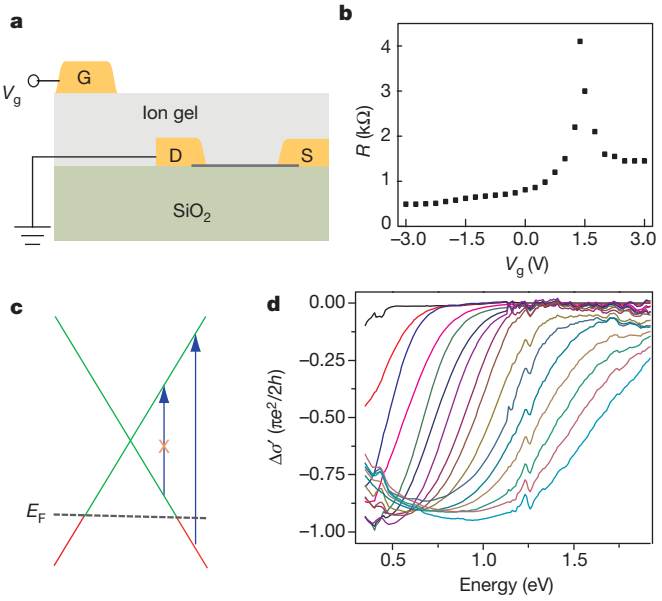

Figure 1 | Controlling the optical transitions in graphene with ion-gel gating. a, Illustration of an ion-gel-gated graphene device on a SiO_2 substrate. G, gate; D, drain; S, source. **b**, Graphene resistance (R) as a function of gate voltage, V_g; R has a maximum at the charge neutral point $V_{CNP} = 1.2$ V. The largest resistance decrease, corresponding to the highest carrier density, occurs at $V_g = -3$ V with hole doping. **c**, Illustration of gate-induced change in graphene absorption. Electronic states are filled (red line) below E_F and empty (green line) above E_F. Electronic transitions (blue arrows) from zero energy to $2|E_F|$ get blocked by hole doping due to empty initial states. **d**, Change in the real part of optical conductivity, $\Delta\sigma'$, when $V_g - V_{CNP}$ is varied from -0.25 to -4 V in steps of 0.25 V. The optical conductivity is reduced for optical excitation energies below $2|E_F|$, which increases with gating strength. $2|E_F|$ values up to 1.8 eV are achieved using the ion-gel gate. (The feature around 1.3 eV is an artefact due to a minimum spectral density of our lamp light source at this energy.)

[1]Department of Physics, University of California at Berkeley, Berkeley, California 94720, USA. [2]Department of Chemical and Biomolecular Engineering, University of California at Berkeley, Berkeley, California 94720, USA. [3]Materials Science Division, Lawrence Berkeley National Laboratory, Berkeley, California 94720, USA.

Report Documentation Page

Form Approved
OMB No. 0704-0188

1. REPORT DATE	2. REPORT TYPE	3. DATES COVERED
31 MAR 2011		**00-00-2011 to 00-00-2011**

4. TITLE AND SUBTITLE	5a. CONTRACT NUMBER
Controlling inelastic light scattering quantum pathways in graphene	5b. GRANT NUMBER
	5c. PROGRAM ELEMENT NUMBER
6. AUTHOR(S)	5d. PROJECT NUMBER
	5e. TASK NUMBER
	5f. WORK UNIT NUMBER
7. PERFORMING ORGANIZATION NAME(S) AND ADDRESS(ES) **University of California at Berkeley,Department of Physics,Berkeley,CA,94720**	8. PERFORMING ORGANIZATION REPORT NUMBER
9. SPONSORING/MONITORING AGENCY NAME(S) AND ADDRESS(ES)	10. SPONSOR/MONITOR'S ACRONYM(S)
	11. SPONSOR/MONITOR'S REPORT NUMBER(S)

12. DISTRIBUTION/AVAILABILITY STATEMENT
Approved for public release; distribution unlimited

13. SUPPLEMENTARY NOTES

14. ABSTRACT

15. SUBJECT TERMS

16. SECURITY CLASSIFICATION OF:			17. LIMITATION OF ABSTRACT	18. NUMBER OF PAGES	19a. NAME OF RESPONSIBLE PERSON
a. REPORT **unclassified**	b. ABSTRACT **unclassified**	c. THIS PAGE **unclassified**	**Same as Report (SAR)**	**4**	

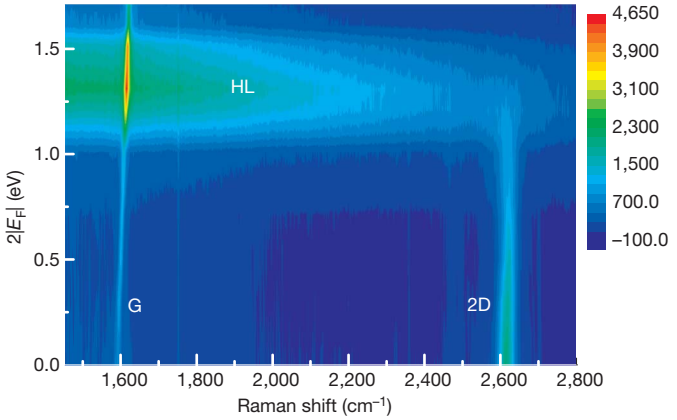

Figure 2 | Controlling inelastic light scattering with electrostatic doping. Graphene inelastic light scattering intensity (colour scale, arbitrary units) is plotted as a function of Stokes Raman redshift and $2|E_F|$ for 1.58-eV laser excitation energy (E_{ex}). G-mode Raman intensity (G; ~1,600 cm^{-1}) is strongly enhanced as $2|E_F|$ approaches E_{ex}, thus blocking some of the Raman quantum pathways. In contrast, the 2D-Raman peak (2D; ~2,600 cm^{-1}) is suppressed and eventually disappears with increasing $2|E_F|$. Broadband hot luminescence (HL) emerges when $2|E_F|$ is lower than but close to E_{ex}.

with reduced optical conductivity below the threshold energy, $2|E_F|$. The transition width of the threshold is due largely to the lifetime broadening from the excited state, and the transition centre yields the $2|E_F|$ value with an uncertainty less than 100 meV. From these spectra, we can also determine the carrier concentration $n = (E_F/\hbar v_F)^2/\pi$ (refs 10, 11), where v_F is the Fermi velocity. With ion-gel gating, vertical electronic transitions with excitation energies as high as 1.8 eV can be blocked. This corresponds to an induced carrier concentration of 6×10^{13} cm^{-2}.

This large gate-induced shift in Fermi energy with ion-gel gating not only allows for controlled optical absorption, but also enables control over inelastic light scattering by varying the allowed intermediate excitations. Using a 785-nm excitation laser (that is, $E_{ex} = 1.58$ eV), we examine the evolution of inelastic light scattering spectra as $2|E_F|$ is varied from 0 to 1.8 eV. Figure 2 shows the inelastic emission intensity as a function of the Raman shift and of $2|E_F|$. At low doping, the spectra are characterized by prominent G-mode (~1,600 cm^{-1}) and 2D-mode (~2,600 cm^{-1}) phonon Raman peaks, as observed in previous studies[12]. But two new features emerge when $2|E_F|$ becomes large enough to significantly alter intermediate-state pathways. (1) With larger $2|E_F|$ blocking part of the Raman quantum pathways, the G-mode Raman intensity does not decrease as one might expect, but increases and reaches a much higher peak value. This behaviour is in contrast to 2D-mode Raman intensity, the intensity of which does decrease monotonically as the resonant Raman pathways are blocked. (2) Photoluminescence over a wide spectral range emerges when $2|E_F|$ is slightly below the laser excitation energy. This hot-electron luminescence from continuous-wave laser excitation is quite unexpected, and it is distinctly different from recently observed nonlinear photoluminescence using femtosecond laser excitations[23,24].

We start our investigation by examining the unusual behaviour of G-mode phonon Raman intensity. The measured Raman peak position Ω_G blue-shifts linearly with Fermi energy as $\Delta\Omega_G = |E_F| \times 42$ cm^{-1} eV^{-1} (Fig. 3a inset). This blue shift is due to phonon renormalization from non-adiabatic electron–phonon coupling, and has been well-studied previously[16,17]. The behaviour of the integrated G-mode Raman intensity with $2|E_F|$ (Fig. 3a), however, has not been observed before. Increased event probability with reduced pathways, as observed in the G-mode Raman intensity here, is a canonical signature of destructive quantum interference. This result highlights the quantum nature of Raman scattering, and provides a valuable probe for microscopic Raman processes in graphene.

G-phonon Raman scattering has been extensively studied for characterizing graphitic materials[12,13,25], and is widely assumed to be a resonant Raman scattering process dominated by pathway I depicted in Fig. 3b (ref. 13). This picture, although appealing, cannot account for our observation. The possibility of enhancement in the Raman G signal on doping because of quantum interference between different Raman pathways was discussed in a recent theoretical study[8]. The

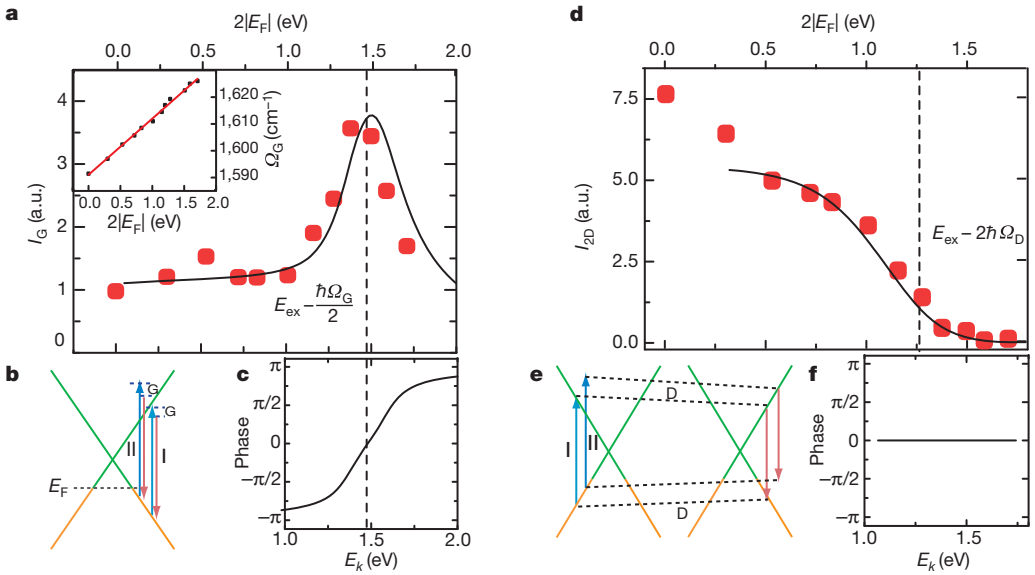

Figure 3 | Quantum interference between graphene Raman pathways. **a**, G-mode Raman intensity as a function of $2|E_F|$ (symbols). A large enhancement is observed when some of the Raman pathways are blocked, which is a hallmark of quantum interference. Black line, theoretical prediction. Inset, doping dependence of G-mode frequency. **b**, Illustration of two representative G-mode Raman pathways (I and II) through two different intermediate excited states. **c**, Quantum phase of Raman pathway amplitude illustrated as a function of intermediate excitation energy. Raman pathways with intermediate excitation energy above and below $E_{ex} - \hbar\Omega_G/2$ (dashed line) have an average phase difference of π and interfere destructively. Blocking pathways below $E_{ex} - \hbar\Omega_G/2$ therefore leads to large enhancement of G-mode Raman scattering. **d**, Doping dependence of 2D-mode Raman intensity (symbols). It drops quickly to zero when $2|E_F|$ approaches $E_{ex} - 2\hbar\Omega_D$ (dashed line), and agrees well with two-phonon Raman scattering theory (black line). **e**, Two representative pathways for the 2D Raman mode. **f**, Two-phonon scattering pathways illustrated in **e** have the same phase and interfere constructively. Blocking these pathways diminishes the intensity of 2D Raman scattering.

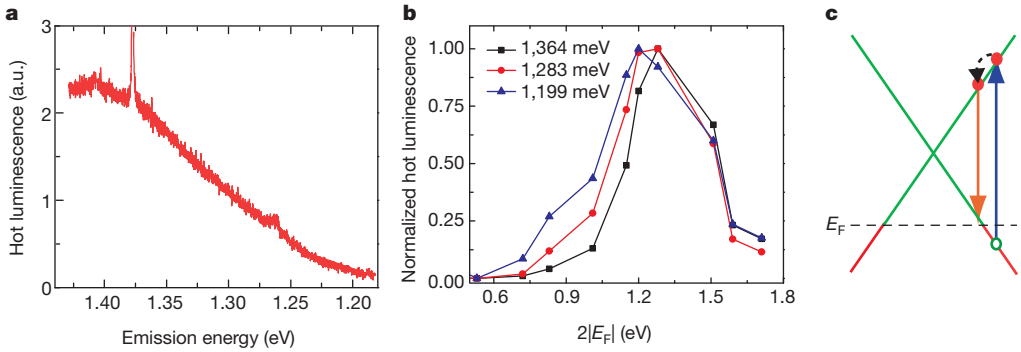

Figure 4 | Hot luminescence in graphene. **a**, Hot luminescence at $2|E_F| = 1.4$ eV shows a broad emission spectrum. It has an integrated intensity (in the range 1.2–1.4 eV) more than 100 times stronger than phonon Raman scattering. **b**, Normalized luminescence intensity as a function of $2|E_F|$ for three different emission energies. Higher energy photon emissions have higher onset values for $2|E_F|$. **c**, Illustration of the hot luminescence generation mechanism. Red and green lines and circles correspond to filled and empty electronic states, respectively. On optical excitation (blue arrow), an excited electron can emit a photon (red arrow) during its relaxation process (dashed arrow), which occurs only if the final valence band state is empty and leads to a broadband emission at energies below $2|E_F|$. Luminescence at a given frequency emerges when $2|E_F|$ approaches the emission energy and disappears when $2|E_F|$ surpasses the excitation energy.

Raman pathways in graphene can be on resonance (I in Fig. 3b), close to resonance (II in Fig. 3b), or off resonance. For a given final state of excitation (that is, emission of an optical phonon with defined momentum and polarization), pathways involving different intermediate states are indistinguishable. Therefore, all the pathways having different quantum mechanical amplitudes (that is, phase and magnitude) will interfere with each other. As such, blocking one quantum pathway can not only decrease but also increase the Raman intensity, depending on its phase relative to other pathways.

G-mode Raman intensity for any specific final one-phonon and one-photon state can be described by[6]:

$$I = \left| \sum_k C_k R_k \right|^2$$

and

$$R_k = \frac{1}{(E_{ex} - E_k - i\gamma)(E_{ex} - \hbar\Omega_G - E_k - i\gamma)}. \quad (1)$$

Here C_k and R_k are the matrix element and resonance factor, respectively, for a Raman pathway through a vertical electronic transition at wavevector k. E_k is the transition energy, E_{ex} the excitation energy, Ω_G the G-phonon frequency, and γ the energy broadening of the excited state. Phase differences between different pathways come mainly from the resonance factor R_k. For example, R_k for pathways resonant with incident light ($E_k = E_{ex}$) and scattered light ($E_k = E_{ex} - \hbar\Omega_G$) have opposite sign for small γ, and their Raman amplitudes largely cancel one other. In Fig. 3c we plot the phase of quantum pathways, $\Phi = \arg(R_k)$, through different intermediate electronic transitions for $E_{ex} = 1.58$ eV. We have set $\gamma = 0.2$ eV, which is estimated from the energy broadening in optical absorption spectra. The phase varies rapidly close to the resonance condition $E_k \approx E_{ex}$. In particular, pathways with transition energy E_k above and below energy $E_{ex} - \hbar\Omega_G/2$ have an average phase difference of π. They interfere destructively if all quantum pathways are allowed, and this leads to a weak overall Raman signal. When $2|E_F|$ is increased to block pathways with transition energies below $E_{ex} - \hbar\Omega_G/2$, the destructive interference is eliminated, and this leads to the observed large enhancement of Raman intensity. When $2|E_F|$ is increased further, more in-phase pathways are blocked and the Raman intensity starts to decrease. A quantitative evaluation of the matrix elements and a summation of all quantum pathways with $\gamma = 0.2$ eV was performed following ref. 8, and the result (black line in Fig. 3a) fits our experimental data (red squares) well. Because the cancellation from destructive interference from different Raman pathways is not perfect with energy dependent transition matrix elements and density of states, the G-mode Raman signal is still observable in undoped graphene. Nevertheless, the Raman intensity with all resonant pathways blocked ($2|E_F| = 1.8$ eV) is approximately the same as when every pathway is allowed ($2|E_F| = 0$). It shows that the simple picture of G-mode graphene Raman scattering, in which only the on-resonance pathways are considered, is invalid.

The integrated intensity of the 2D-mode Raman peak, which results from simultaneous excitation of two phonons with wavevector close to the K-point in the graphene Brillouin zone, exhibits a doping dependence completely different from that of the integrated intensity of the G-mode Raman peak. Figure 3d shows the 2D-mode Raman intensity as a function of $2|E_F|$. The 2D intensity decreases slowly with increased doping when $2|E_F|$ is relatively small, which was observed previously[14] and can be explained theoretically through the excited state broadening[14,26]. Here we focus on the behaviour when $2|E_F|$ approaches E_{ex}. Instead of an enhanced scattering intensity as in G-mode Raman, the 2D-mode intensity drops quickly at the threshold energy $2|E_F| = E_{ex} - 2\hbar\Omega_D$, where Ω_D is the zone-boundary phonon frequency.

The intensity of 2D-mode Raman scattering is also determined by quantum interference between different pathways. Figure 3e illustrates two representative Raman pathways, including one satisfying the double resonance condition (pathway I)[12]. Such two-phonon Raman pathways have one more virtual transition than one-phonon processes, and it has a profound effect on the Raman interference behaviour. Quantitatively, quantum interference in 2D-mode Raman for a specific final two-phonon and one-photon state is described by[6]:

$$I = \left| \sum_k D_k R_k \right|^2, \quad (2)$$

$$R_k = \frac{1}{(E_{ex} - E_k - i\gamma)(E_{ex} - \hbar\Omega_D - E_{k'} - i\gamma)(E_{ex} - 2\hbar\Omega_D - E_{k''} - i\gamma)}$$

Here D_k is the matrix element of 2D-mode Raman scattering for a pathway starting at transition k. E_k, $E_{k'}$ and $E_{k''}$ are the energies of the three intermediate states. The resonance factor R_k determines the relative phase between different pathways. Figure 3f plots the phase of quantum pathways, involving the emission of two phonons with a specific wavevector, as a function of first-intermediate-state energy E_k for processes similar to those depicted in Fig. 3e (see also Supplementary Information). All the different pathways have the same phase and they interfere constructively. As a result, any reduction in quantum pathways leads to decreased Raman intensity, and when all resonant channels are blocked, the 2D-mode Raman signal becomes negligible. In Fig. 3d we show a more quantitative comparison between this theoretical picture (black line) and experimental results (symbols).

Last, we examine the graphene hot luminescence. Figure 4a shows the hot luminescence spectrum at $2|E_F| = 1.4$ eV, which is characterized by a broadband emission. To investigate the effect of carrier doping, we plot in Fig. 4b the normalized luminescence intensity as a function of

$2|E_F|$ for several emission energies (symbols). The luminescence is distinctly different from electronic Raman scattering[27] because zero-momentum electron–hole pair excitations required for the electronic Raman scattering do not exist in the strongly doped graphene. The peak observed in the hot luminescence when $2|E_F|$ approaches E_{ex} also has a different physical origin compared with that in G-mode phonon Raman. Instead of being an interference phenomenon from blocked Raman quantum pathways, the hot luminescence maximum is a consequence of newly opened dynamic pathways for photo-excited hot carriers.

We depict this dynamic process in Fig. 4c. An incident photon generates an electron and a hole, which then relax to the Fermi level through interactions with low-energy electrons and phonons. During the relaxation process, a hot electron has a finite probability of emitting a photon, but requires the final valence band state to be empty because of Pauli blocking (Fig. 4c). This pathway is opened up only when $2|E_F|$ exceeds the light emission energy, and defines a threshold doping level for hot luminescence generation. The qualitative features observed in Fig. 4b can be understood using this picture: hot luminescence emerges when the energy $2|E_F|$ is higher than an onset value that increases with the emission photon energy. When $2|E_F|$ is further increased to a value greater than the laser energy, hot luminescence at all energies suddenly disappears as the initial photoexcitations are blocked. Because the hot luminescence arises from radiative decay of excited electrons right after photoexcitation, it could become a valuable probe for ultrafast electron dynamics in graphene[9].

Our study shows that inelastic light scattering phenomena can be explored by controlling the intermediate excited states. In graphene, it enables us to demonstrate the critical role of quantum interference in Raman scattering, and to reveal a new broadband hot luminescence. Such inelastic light scattering control could also be applied to general nanoscale material research, because electronic transitions in many nanostructures can be modified in a controlled fashion (for example, electrostatic gating of carbon nanotubes[28] and electrochemically tuned semiconductor quantum dots[29]). This control will make inelastic light scattering a more powerful tool for probing novel nanoscale physics. It could also lead to optimized inelastic light scattering in nanomaterials for biological sensors and optoelectronic applications.

METHODS SUMMARY

In this study we use large area graphene grown by chemical vapour deposition[30]. Graphene is grown on copper films using CH_4 as the feed gas, which was then transferred with poly(methyl methacrylate) (PMMA) support to a fused silica substrate after wet-etching to remove the copper film by $FeCl_3$. The PMMA support is dissolved in acetone solution. Subsequently, Ti (10 nm) and Au (40 nm) were deposited in vacuum through stencil masks onto the graphene sample for the source, drain and gate electrodes.

The ionic liquid, 1-ethyl-3-methylimidazolium bis(trifluoromethylsulphonyl)imide ([EMIM][TFSI]), was purchased from EMD Chemicals. The ionic liquid was dried at $T = 100\ ^{\circ}C$ under vacuum ($\sim$200 mtorr) for 3 days and then transferred to an inert-atmosphere glove box. Polystyrene-*b*-poly(ethylene oxide)-*b*-polystyrene (PS-PEO-PS) triblock copolymer was purchased from Polymer Source and used as received. The quoted molecular weights of the block copolymer moieties were 10-44-10 kg mol^{-1} for the PS-PEO-PS blocks, respectively (PEO volume fraction = 0.67). The physically crosslinked, ionic liquid/triblock copolymer gel (ion gel) was produced in the following manner. In an inert atmosphere glove box, 0.55 g of [EMIM][TFSI] were dissolved with 21 mg of PS-PEO-PS in 2 ml of dry dichloromethane. The solution was stirred overnight at room temperature. The ion gel was removed from the glove box and spin-coated on the graphene sample at a rate of 4,000 r.p.m.

Infrared transmission measurements were performed with a Fourier transform infrared spectrometer at the Advanced Light Source, Lawrence Berkeley National Laboratory. Inelastic light scattering was measured with a micro-Raman set-up with a 785-nm excitation laser. The Raman set-up has a spectral resolution of 1 cm^{-1}. All measurements were performed in air and at 300 K.

Received 1 September 2010; accepted 18 January 2011.
Published online 16 March 2011.

1. Raman, C. V. A change of wave-length in light scattering. *Nature* **121,** 619 (1928).
2. Landsberg, G. & Mandelstam, L. Eine neue Erscheinung bei der Lichtzerstreuung in Krystallen. *Naturwissenschaften* **16,** 557 (1928).
3. Rao, A. M. *et al.* Diameter-selective Raman scattering from vibrational modes in carbon nanotubes. *Science* **275,** 187–191 (1997).
4. Devereaux, T. P. & Hackl, R. Inelastic light scattering from correlated electrons. *Rev. Mod. Phys.* **79,** 175–233 (2007).
5. Goñi, A. R. *et al.* One-dimensional plasmon dispersion and dispersionless intersubband excitations in GaAs quantum wires. *Phys. Rev. Lett.* **67,** 3298–3301 (1991).
6. Cardona, M. *Light Scattering in Solids I* 2nd edn (Springer, 1982).
7. Ralston, J. M., Wadsack, R. L. & Chang, R. K. Resonant cancelation of Raman scattering from CdS and Si. *Phys. Rev. Lett.* **25,** 814–818 (1970).
8. Basko, D. M. Calculation of the Raman G peak intensity in monolayer graphene: role of Ward identities. *N. J. Phys.* **11,** 095011 (2009).
9. Elsaesser, T., Shah, J., Rota, L. & Lugli, P. Initial thermalization of photoexcited carriers in GaAs studied by femtosecond luminescence spectroscopy. *Phys. Rev. Lett.* **66,** 1757–1760 (1991).
10. Novoselov, K. S. *et al.* Two-dimensional gas of massless Dirac fermions in graphene. *Nature* **438,** 197–200 (2005).
11. Zhang, Y. B., Tan, Y. W., Stormer, H. L. & Kim, P. Experimental observation of the quantum Hall effect and Berry's phase in graphene. *Nature* **438,** 201–204 (2005).
12. Ferrari, A. C. *et al.* Raman spectrum of graphene and graphene layers. *Phys. Rev. Lett.* **97,** 187401 (2006).
13. Pimenta, M. A. *et al.* Studying disorder in graphite-based systems by Raman spectroscopy. *Phys. Chem. Chem. Phys.* **9,** 1276–1291 (2007).
14. Das, A. *et al.* Monitoring dopants by Raman scattering in an electrochemically top-gated graphene transistor. *Nature Nanotechnol.* **3,** 210–215 (2008).
15. Dresselhaus, M. S., Jorio, A., Hofmann, M., Dresselhaus, G. & Saito, R. Perspectives on carbon nanotubes and graphene Raman spectroscopy. *Nano Lett.* **10,** 751–758 (2010).
16. Pisana, S. *et al.* Breakdown of the adiabatic Born-Oppenheimer approximation in graphene. *Nature Mater.* **6,** 198–201 (2007).
17. Yan, J., Zhang, Y. B., Kim, P. & Pinczuk, A. Electric field effect tuning of electron-phonon coupling in graphene. *Phys. Rev. Lett.* **98,** 166802 (2007).
18. Li, Z. Q. *et al.* Dirac charge dynamics in graphene by infrared spectroscopy. *Nature Phys.* **4,** 532–535 (2008).
19. Wang, F. *et al.* Gate-variable optical transitions in graphene. *Science* **320,** 206–209 (2008).
20. Zhang, Y. *et al.* Direct observation of a widely tunable bandgap in bilayer graphene. *Nature* **459,** 820–823 (2009).
21. Cho, J. H. *et al.* Printable ion-gel gate dielectrics for low-voltage polymer thin-film transistors on plastic. *Nature Mater.* **7,** 900–906 (2008).
22. Kim, B. J. *et al.* High-performance flexible graphene field effect transistors with ion gel gate dielectrics. *Nano Lett.* **10,** 3464–3466 (2010).
23. Lui, C. H., Mak, K. F., Shan, J. & Heinz, T. F. Ultrafast photoluminescence from graphene. Preprint at ⟨http://arXiv.org/abs/1006.5769⟩ (2010).
24. Stoehr, R. J., Kolesov, R., Pflaum, J. & Wrachtrup, J. Fluorescence of laser created electron-hole plasma in graphene. Preprint at ⟨http://arXiv.org/abs/1006.5434⟩ (2010).
25. Dresselhaus, M. S., Dresselhaus, G., Saito, R. & Jorio, A. Raman spectroscopy of carbon nanotubes. *Phys. Rep.* **409,** 47–99 (2005).
26. Basko, D. M., Piscanec, S. & Ferrari, A. C. Electron-electron interactions and doping dependence of the two-phonon Raman intensity in graphene. *Phys. Rev. B* **80,** 165413 (2009).
27. Kashuba, O. & Fal'ko, V. I. Signature of electronic excitations in the Raman spectrum of graphene. *Phys. Rev. B* **80,** 241404(R) (2009).
28. Ilani, S., Donev, L. A. K., Kindermann, M. & McEuen, P. L. Measurement of the quantum capacitance of interacting electrons in carbon nanotubes. *Nature Phys.* **2,** 687–691 (2006).
29. Wang, C. J., Shim, M. & Guyot-Sionnest, P. Electrochromic nanocrystal quantum dots. *Science* **291,** 2390–2392 (2001).
30. Li, X. S. *et al.* Large-area synthesis of high-quality and uniform graphene films on copper foils. *Science* **324,** 1312–1314 (2009).

Supplementary Information is linked to the online version of the paper at www.nature.com/nature.

Acknowledgements This work was supported by the US Department of Energy, Laboratory Directed Research and Development Program of Lawrence Berkeley National Laboratory under contract no. DE-AC02-05CH11231 (C.-F.C. and F.W.), by the Office of Basic Energy Sciences under contract nos DE-AC02-05CH11231 (B.W.B. and R.A.S.), DE-AC03-76SF0098 (Materials Science Division) (C.G., A.Z.) and DE-AC02-05CH11231 (Advanced Light Source), and by ONR MURI award N00014-09-1-1066 (J.H., C.-H.P., S.G.L., M.F.C.). C.-F.C. also acknowledges fellowship support from the National Science Council and National Tsing Hua University, Taiwan, under awards NSC98-2811-M-007-008 and NSC98-2120-M-007-004.

Author Contributions F.W. designed the experiment; C.-F.C. and J.H. carried out optical measurements; B.G., C.G. and B.W.B. contributed to sample growth and fabrication; and C.-H.P., S.G.L. and F.W. performed theoretical analysis. All authors discussed the results and wrote the paper together.

Author Information Reprints and permissions information is available at www.nature.com/reprints. The authors declare no competing financial interests. Readers are welcome to comment on the online version of this article at www.nature.com/nature. Correspondence and requests for materials should be addressed to F.W. (fengwang76@berkeley.edu).